Light-powered Self-excited Coupled Oscillators in Huygens ' Synchrony

Quanbao Cheng
Anhui Jianzhu University
Kai Li (kli@ahjzu.edu.cn)
Anhui Jianzhu University https://orcid.org/0000-0003-4898-2827

Research Article

Keywords: Self-excited motion, Liquid crystal elastomer, In-phase synchronization, Anti-phase synchronization, Domain of attract

Posted Date: May 11th, 2021

DOI: https://doi.org/10.21203/rs.3.rs-494050/v1

Light-powered self-excited coupled oscillators in Huygens' synchrony

Quanbao Cheng, Kai Li*

Department of Civil Engineering, Anhui Jianzhu University, Hefei, Anhui 230601, China

Abstract

Self-excited motions have the advantages of actively collecting energy from the environment, autonomy, making equipment portable and so on, and a great number of self-excited motion modes have recently been developed which greatly expand the application in active machines. However, there are few studies on the synchronization and group behaviors of self-excited coupled oscillators, which are common in nature. Based on light-powered self-excited oscillator composed of liquid crystal elastomer (LCE) bars, the synchronization of two self-excited coupled oscillators is theoretically studied. Numerical calculations show that self-excited oscillations of the system have two synchronization modes: in-phase mode and anti-phase mode. The time histories of various quantities are calculated to elucidate the mechanism of self-excited oscillation and synchronization. Furthermore, the effects of initial conditions and interaction on the two synchronization modes of the self-excited oscillation are investigated extensively. For strong interactions, the system always develops into in-phase synchronization mode, while for weak interaction, the system will evolve into anti-phase synchronization mode. Meanwhile, the initial condition generally does not affect the synchronization mode and its amplitude. This work will deepen people's understanding of synchronization behaviors of self-excited coupled oscillators, and provide promising applications in energy harvesting, signal monitoring, soft robotics and medical equipment.

Keywords: Self-excited motion; Liquid crystal elastomer; In-phase synchronization; Anti-phase synchronization; Domain of attraction.

---

*Corresponding author. E-mail address: kli@ahjzu.edu.cn (K. Li).

1 Introduction

Self-excited oscillation is a phenomenon of periodic state change of system under constant external stimulation [1-6], and has wide application prospects in many fields, such as energy harvesting, signal monitoring, soft robotics and medical equipment [7-11], because of its unique advantages. First, self-excited oscillation of the system can directly collect energy from the constant external environment for maintaining its periodic motion, which is similar to the effect of biological active feeding. Second, the periodic motion of self-excited oscillation does not need periodic external stimulation, only constant external stimulation. This feature greatly reduces the requirement of system motion control, and does not need to design a complex controller. Third, the above characteristics of no controller and battery greatly reduce the complexity of the active machine and make it more portable, which is expected to achieve high power [10-13]. In many conventional and active material systems, different self-excited oscillations have been constructed recently[14-18].

In nonconservative oscillation, the energy loss of self-excited oscillation caused by system damping needs external energy input and energy compensation [8,14-20]. Recently, based on different stimuli-responsive materials and structures, different feedback mechanisms are proposed to realize energy compensation [14,15,18]. The stimuli-responsive materials for self-excited oscillation systems include hydrogels, ionic gels, liquid crystal elastomer (LCE) and so on. Meanwhile, different feedback mechanisms include coupling of chemical reaction and large deformation [19,20], self-shading effect [14,15], multi-process coupling of droplet evaporation and plate bending [8]. Self-excited oscillations come from the nonlinear coupling of multiple processes of the system. Among the stimuli-responsive materials, LCE has the advantages of fast response, recoverable deformation and low noise [21,22]. LCE is a polymer network structure formed by cross-linking liquid crystal monomer molecules. Under the stimulation of external fields, such as light, heat, electricity and magnetism, the liquid crystal monomer molecules will rotate or undergo phase transition, and change the configuration to induce macroscopic deformation [22]. A lot of experimental and theoretical work has been done on self-excited oscillations

based on LCE [14-18,23-32].

Although a lot of work has been done on single self-excited oscillator, the interaction and collective motion of multiple self-excited oscillators need to be further explored. Synchronization and collective motion are ubiquitous in nature, such as the circadian rhythm and the cardiac pacemaker cells [33-36]. The first work on synchronization can be traced back to Huygens' observation on the synchronization of coupled pendulums in 1665 [37]. He observed that two identical clocks oscillate synchronously with two pendulums in opposite directions. Recent studies have confirmed that the synchronization between two pendulums results from the coupling caused by small mechanical vibrations that propagate in the wooden structure connecting the clocks [38]. Furthermore, the synchronous movement of a large number of metronomes with more degrees of freedom on a free moving base is also realized experimentally [39]. Recently, based on light-responsive LCE, Ghislaine et al. experimentally studied the synchronized oscillations of thin plastic actuators fueled by light, and found two kinds of synchronous oscillation phenomena of in-phase and anti-phase in steady state [40]. Their numerical simulations qualitatively explain the origin of the synchronized motion, and found that the motion can be tuned by the mechanical properties of the coupling joint.

At present, there are few studies on the interaction and group phenomenon of self-excited coupled oscillators based on active materials [40], and the synchronization mechanism and its behavior need to be further explored. In this paper, based on the self-excited oscillator of photoresponsive LCE proposed previously by us [41], we investigate the synchronous behavior of two identical self-excited oscillators powered by steady illumination. This paper is as follows. Firstly, based on dynamic LCE model [42], the dynamic governing equation for two identical self-excited oscillators under steady illumination is formulated in Sec. 2. Secondly, two kinds of synchronization mode of the self-excited oscillations are presented in Sec. 3. In Sec. 4 and 5, ,the detailed self-excited mechanism of in-phase and anti-phase modes are elucidated, respectively. Meanwhile, the influences of initial conditions and spring constant on the synchronization mode, amplitude and

period of the self-excited oscillations are investigated. Finally, the conclusion is given in Sec. 6.

2 Model and formulation

2.1 Dynamic model of the two LCE oscillators

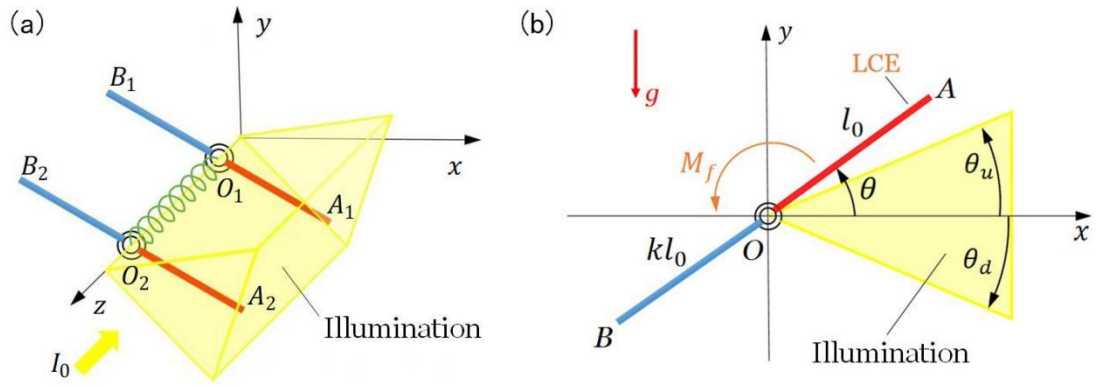

Fig. 1 Schematics of dynamic model of two identical LCE oscillators connected by a torsion spring under steady illumination. The LCE oscillators are made up of a light-responsive LCE bar and a regular material bar. The region from θ_{d} to θ_{u} is steadily illuminated.

Fig. 1a sketches the dynamic model of two identical LCE oscillators connected by a torsion spring under steady illumination. O_1A_1 and O_2A_2 are light-responsive LCE bars, while O_1B_1 and O_2B_2 are conventional bars. The four bars have the same mass m. $A_1O_1B_1$ and $A_2O_2B_2$ bars can rotate around the z axis. The original length of O_1A_1 and O_2A_2 are l_0, and the length of O_1B_1 and O_2B_2 are kl_0, with k being the length ratio. The connecting torsion spring between the two bars can apply corresponding torque to each other, which depends on the relative angle difference between the two bars. The illumination zone is denoted by the upper edge angle θ_{u} and the lower edge angle θ_{d}, as shown in Fig. 1b. The positions of O_1A_1 and O_2A_2 are denoted by θ_1 and θ_2, respectively. The initial angles of O_1A_1 and O_2A_2 are θ_1^0 and θ_2^0, respectively. The initial angular velocity is of O_1A_1 and O_2A_2

are $\dot{\theta}_1^0$ and $\dot{\theta}_2^0$, respectively. Under light illumination, O_1A_1 bar and O_2A_2 bar can oscillate, because the light-driven deformation periodically changes the center of gravity and reverse the resultant moment of the system due to self-shadowing effect. In the following, we will investigate the synchronization of the two self-excited oscillations.

According to the theorem of moment of momentum, the differential equations for the dynamics of the two LCE bars rotating around the fixed z axis are

$$\frac{\mathrm{d}\Psi_1}{\mathrm{d}t} = M_{z1}, \quad \frac{\mathrm{d}\Psi_2}{\mathrm{d}t} = M_{z2}, \tag{1}$$

where the angular momenta of $A_1O_1B_1$ and $A_2O_2B_2$ are , respectively,

$$\Psi_1 = J_{z1}(t)\frac{\mathrm{d}\theta_1(t)}{\mathrm{d}t}, \quad \Psi_2 = J_{z2}(t)\frac{\mathrm{d}\theta_2(t)}{\mathrm{d}t}, \tag{2}$$

where the moments of inertia of $A_1O_1B_1$ and $A_2O_2B_2$ about z axis are, respectively,

$$J_{z1} = J_{A1} + J_{B1}, \quad J_{z2} = J_{A2} + J_{B2}, \tag{3}$$

where $J_{A1} = \frac{1}{3}ml_1^2$ is the moment of inertia of O_1A_1 about z axis, $J_{B1} = \frac{1}{3}mk^2{l_0}^2$ is the moment of inertia of O_1B_1 about z axis, $J_{A2} = \frac{1}{3}ml_2^2$ is the moment of inertia of O_2A_2 about z axis, and $J_{B2} = \frac{1}{3}mk^2{l_0}^2$ is the moment of inertia of O_2B_2 about z axis. It is worth noting that the length depends on the light-driven contraction strain. Then, the length l_1 of the O_1A_1 and the length l_2 of the O_2A_2 can be expressed as

$$l_1 = [1 + \varepsilon_1(\mathrm{t})]l_0, \quad l_2 = [1 + \varepsilon_2(\mathrm{t})]l_0, \tag{4}$$

where $\varepsilon_1(t)$ and $\varepsilon_2(t)$ are the light-driven contraction strains of O_1A_1 and O_2A_2, respectively. For simplicity, we assume that the light-driven contraction strain of the material is proportional to the number fraction $\varphi(t)$,

$$\varepsilon_1(t) = -C_0\varphi_1(t), \quad \varepsilon_2(t) = -C_0\varphi_2(t), \tag{5}$$

where C_0 is the contraction coefficient. The number fraction $\varphi(t)$ will be given in

Sec. 2.2.

In Eq. (1), M_{z1} and M_{z2} are the resultant moments of all external forces of bar $A_1O_1B_1$ and bar $A_2O_2B_2$ to *z*-axis, respectively,

$$M_{z1} = M_{D1} - M_{f1} + M_K, \quad M_{z2} = M_{D2} - M_{f2} - M_K, \tag{6}$$

where, the driving moments of $A_1O_1B_1$ and $A_2O_2B_2$ can easily be calculated as

$$M_{D1} = \frac{1}{2}mg\left(kl_0\cos\theta_1 - l_1\cos\theta_1\right), \quad M_{D2} = \frac{1}{2}mg\left(kl_0\cos\theta_2 - l_2\cos\theta_2\right), \tag{7}$$

where g is the gravitational acceleration.

The damping force is assumed to be proportional to the velocity, and then the damping moments of $A_1O_1B_1$ and $A_2O_2B_2$ can be easily calculated as

$$M_{f1} = \frac{1}{3}\beta\left(l_1^3 + k^3l_0^3\right)\frac{\mathrm{d}\theta_1}{\mathrm{d}t}, \quad M_{f2} = \frac{1}{3}\beta\left(l_2^3 + k^3l_0^3\right)\frac{\mathrm{d}\theta_2}{\mathrm{d}t}, \tag{8}$$

where β is the damping coefficient, $\frac{\mathrm{d}\theta_1}{\mathrm{d}t} = \dot{\theta}_1$ is the angular velocity of $A_1O_1B_1$ and $\frac{\mathrm{d}\theta_2}{\mathrm{d}t} = \dot{\theta}_2$ is the angular velocity of $A_2O_2B_2$.

The moment exerted by the torsion spring on the two bars is assumed to be linear with the angle difference,

$$M_K = \alpha\left(\theta_1 - \theta_2\right), \tag{9}$$

where α is the spring coefficient of the torsion spring.

2.2 Evolution law of number fraction in the two LCE oscillators

In order to calculate the light-driven contraction strain and the lengths of the LCE bars, we need to obtain the number fractions in the LCE bars. According to the research of Yu et al., the *trans*-to-*cis* isomerization of LCE can be induced by UV or laser with wavelength less than 400 nm [43]. Generally, the *cis*-to-*trans* isomerization driven by UV light and the thermal *trans*-to-*cis* excitation can be neglected. Therefore, the number fraction of *cis* isomers depends on the thermal excitation from *trans* to *cis*, the thermally driven relaxation from *cis* to *trans* and the light-driven *trans*-to-*cis* isomerization. Then, the number fraction of bent *cis* isomers in LCE can be governed by the following equation [42, 43],

$$\frac{\partial \varphi}{\partial t} = \eta_0 I_0 (1-\varphi) - \frac{\varphi}{T_0}, \tag{10}$$

where T_0 is the thermal relaxation time of *cis* state to *trans* state, I_0 is the light intensity, and η_0 is the light absorption constant. By solving Eq. (10), the number fraction of *cis*-isomers can be expressed as:

$$\varphi(t) = \frac{\eta_0 T_0 I_0}{\eta_0 T_0 I_0 + 1} + (\varphi_0 - \frac{\eta_0 T_0 I_0}{\eta_0 T_0 I_0 + 1}) \exp\left[-\frac{t}{T_0} (\eta_0 T_0 I_0 + 1) \right], \tag{11}$$

where φ_0 is the number fraction of *cis* isomers at $t = 0$. In the light zone, for initially zero number fraction of *cis* isomers, i.e., $\varphi_0 = 0$, Eq. (11) can be simplified as

$$\varphi(t) = \frac{\eta_0 T_0 I_0}{\eta_0 T_0 I_0 + 1} \left\{ 1 - \exp\left[-\frac{t}{T_0} \left(1 + \eta_0 T_0 I_0 \right) \right] \right\}. \tag{12}$$

In the dark zone, namely $I_0 = 0$, φ_0 can be set as the maximum value of $\varphi(t)$ in Eq. (12), namely, $\varphi_0 = \frac{\eta_0 T_0 I_0}{\eta_0 T_0 I_0 + 1}$, and Eq. (11) can be simplified as:

$$\varphi(t) = \frac{\eta_0 T_0 I_0}{\eta_0 T_0 I_0 + 1} \exp\left(-\frac{t}{T_0} \right). \tag{13}$$

By defining the following dimensionless quantities: $\bar{t} = t / T_0$, $\bar{I} = \eta_0 T_0 I_0$, $\bar{g} = \left(T_0 / \sqrt{l_0 / g} \right)^2$, $\bar{\beta} = 2 \beta l_0 T_0 / m$, $\bar{\alpha} = \alpha T_0^2 / \left(m l_0^2 \right)$, $\bar{\varphi} = \varphi \left(\eta_0 T_0 I_0 + 1 \right) / \eta_0 T_0 I_0$, $\bar{M}_K = M_K T_0^2 / \left(m l_0^2 \right)$, $\bar{M}_{D1} = 2 M_{D1} T_0^2 / \left(m l_0^2 \right)$ and $\bar{M}_{D2} = 2 M_{D2} T_0^2 / \left(m l_0^2 \right)$, in the light zone, Eq. (12) is rewritten as:

$$\bar{\varphi} = 1 - \exp\left[-\bar{t} (\bar{I} + 1) \right], \tag{14}$$

in the dark zone, Eq. (13) becomes:

$$\bar{\varphi} = \exp(-\bar{t}). \tag{15}$$

2.3 Governing equation for movement of the LCE oscillators

A combination of Eqs. (1)-(4), (14) and (15) can yield,

in the light zone:

$$\frac{\mathrm{d}^2\theta_1}{\mathrm{d}\bar{t}_1^2}=\frac{4C_0\bar{I}(1+\varepsilon_1)\exp\left[-\bar{t}_1(\bar{I}+1)\right]-\bar{\beta}\left[(1+\varepsilon_1)^3+k^3\right]}{2(1+\varepsilon_1)^2+2k^2}\frac{\mathrm{d}\theta_1}{\mathrm{d}\bar{t}_1}+\frac{3\bar{g}(k-\varepsilon_1-1)\cos\theta_1-6\bar{\alpha}(\theta_1-\theta_2)}{2(1+\varepsilon_1)^2+2k^2}, \tag{16}$$

$$\frac{\mathrm{d}^2\theta_2}{\mathrm{d}\bar{t}_2^2}=\frac{4C_0\bar{I}(1+\varepsilon_2)\exp\left[-\bar{t}_2(\bar{I}+1)\right]-\bar{\beta}\left[(1+\varepsilon_2)^3+k^3\right]}{2(1+\varepsilon_2)^2+2k^2}\frac{\mathrm{d}\theta_2}{\mathrm{d}\bar{t}_2}+\frac{3\bar{g}(k-\varepsilon_2-1)\cos\theta_2+6\bar{\alpha}(\theta_1-\theta_2)}{2(1+\varepsilon_2)^2+2k^2}, \tag{17}$$

where $\varepsilon_1=-C_0\bar{I}\left\{1-\exp\left[-\bar{t}_1(\bar{I}+1)\right]\right\}/(\bar{I}+1)$ and $\varepsilon_2=-C_0\bar{I}\left\{1-\exp\left[-\bar{t}_2(\bar{I}+1)\right]\right\}/(\bar{I}+1)$,

in the dark zone:

$$\frac{\mathrm{d}^2\theta_1}{\mathrm{d}\bar{t}_1^2}=\frac{-4C_0\bar{I}(1+\varepsilon_1)\exp(-\bar{t}_1)-\bar{\beta}\left[(1+\varepsilon_1)^3+k^3\right]}{2(1+\varepsilon_1)^2+2k^2}\frac{\mathrm{d}\theta_1}{\mathrm{d}\bar{t}_1}+\frac{3\bar{g}(k-\varepsilon_1-1)\cos\theta_1-6\bar{\alpha}(\theta_1-\theta_2)}{2(1+\varepsilon_1)^2+2k^2}, \tag{18}$$

$$\frac{\mathrm{d}^2\theta_2}{\mathrm{d}\bar{t}_2^2}=\frac{-4C_0\bar{I}(1+\varepsilon_2)\exp(-\bar{t}_2)-\bar{\beta}\left[(1+\varepsilon_2)^3+k^3\right]}{2(1+\varepsilon_2)^2+2k^2}\frac{\mathrm{d}\theta_2}{\mathrm{d}\bar{t}_2}+\frac{3\bar{g}(k-\varepsilon_2-1)\cos\theta_2+6\bar{\alpha}(\theta_1-\theta_2)}{2(1+\varepsilon_2)^2+2k^2}, \tag{19}$$

where $\varepsilon_1=-C_0\bar{I}\exp(-\bar{t}_1)/(\bar{I}+1)$ and $\varepsilon_2=-C_0\bar{I}\exp(-\bar{t}_2)/(\bar{I}+1)$.

2.4 Solution method

Eqs. (16)-(19) are ordinary differential equations with variable coefficients, and there are no analytic solutions. Hereon, the classical fourth-order Runge-Kutta method is utilized to solve ordinary differential equations by *Matlab* software. We transform the second-order ordinary differential equation into first-order ordinary differential equations:

$$\begin{cases}\dfrac{\mathrm{d}\theta_1}{\mathrm{d}\bar{t}}=f_1\left(\bar{t},\theta_1,\dot{\theta}_1,\theta_2,\dot{\theta}_2\right)\\ \dfrac{\mathrm{d}\dot{\theta}_1}{\mathrm{d}\bar{t}}=f_2\left(\bar{t},\theta_1,\dot{\theta}_1,\theta_2,\dot{\theta}_2\right)\\ \dfrac{\mathrm{d}\theta_2}{\mathrm{d}\bar{t}}=f_3\left(\bar{t},\theta_1,\dot{\theta}_1,\theta_2,\dot{\theta}_2\right)\\ \dfrac{\mathrm{d}\dot{\theta}_2}{\mathrm{d}\bar{t}}=f_4\left(\bar{t},\theta_1,\dot{\theta}_1,\theta_2,\dot{\theta}_2\right)\end{cases}. \tag{20}$$

The initial conditions are as follows:

$$\begin{cases} \theta_1(\bar{t}=0)=\theta_1^0 \\ \dot{\theta}_1(\bar{t}=0)=\dot{\theta}_1^0 \\ \theta_2(\bar{t}=0)=\theta_2^0 \\ \dot{\theta}_2(\bar{t}=0)=\dot{\theta}_2^0 \end{cases}. \tag{21}$$

By defining the following vectors $\boldsymbol{y}=(\theta_1,\dot{\theta}_1,\theta_2,\dot{\theta}_2)^{\mathrm{T}}$, $\boldsymbol{y_0}=(\theta_1^0,\dot{\theta}_1^0,\theta_2^0,\dot{\theta}_2^0)^{\mathrm{T}}$, and $\boldsymbol{f}=(f_1,f_2,f_3,f_4)^{\mathrm{T}}$, Eqs. (20) and (21) can be expressed as follows:

$$\begin{cases} \mathbf{y}'=\mathbf{f}(\bar{t},\mathbf{y}) \\ \mathbf{y}(\bar{t}=0)=\mathbf{y}_0 \end{cases}. \tag{22}$$

Following the classical fourth-order Runge-Kutta method, Eq. (22) can be written as,

$$\mathbf{y}_{n+1}=\mathbf{y}_n+\frac{H}{6}(\mathbf{k}_1+2\mathbf{k}_2+2\mathbf{k}_3+\mathbf{k}_4), \tag{23}$$

where H is the time step, and $\mathbf{k}_i$ (i =1 to 4) are listed as below,

$$\begin{cases} \mathbf{k}_1=\mathbf{f}(\bar{t}_n,\mathbf{y}_n) \\ \mathbf{k}_2=\mathbf{f}\left(\bar{t}_n+\frac{H}{2},\mathbf{y}_n+\frac{H}{2}\mathbf{k}_1\right) \\ \mathbf{k}_3=\mathbf{f}\left(\bar{t}_n+\frac{H}{2},\mathbf{y}_n+\frac{H}{2}\mathbf{k}_2\right) \\ \mathbf{k}_4=\mathbf{f}(\bar{t}_n+H,\mathbf{y}_n+H\mathbf{k}_3) \end{cases}. \tag{24}$$

The self-excited motion of the LCE oscillators, i.e., the variation of angle and angular velocity with time, can be obtained by iteration.

3 Two synchronization modes

Fig 2 shows two typical synchronization modes of self-excited motion of the LCE oscillators: in-phase mode and anti-phase mode. In the computation, we fix $\bar{I}=0.25$, $C_0=0.4$, $\bar{g}=9.8$, $k=9.2$, $\bar{\beta}=0.882$, $\dot{\theta}_1^0=-0.33$, $\dot{\theta}_2^0=0.33$, $\theta_u=45°$, $\theta_d=-80°$, $\theta_1^0=0°$ and $\theta_2^0=10°$. The time-history curve and domain of attraction of the in-phase mode for $\bar{\alpha}=0.1$ are given in Figs. 2a and c, respectively. The results show that the two LCE bars oscillate in-phase. Figs. 2b and d present the time-history curve and domain of attraction of the anti-phase mode for $\bar{\alpha}=0.03$, respectively. The results show that the two LCE bars oscillate in anti-phase mode. Through careful calculation, it is found that there exists a critical spring constant $\bar{\alpha}_{\mathrm{crit}}=0.075$ for the two synchronization modes. The two LCE oscillators will oscillate in in-phase mode

for $\overline{\alpha} > \overline{\alpha}_{\text{crit}}$, while oscillate in anti-phase mode for $\overline{\alpha} < \overline{\alpha}_{\text{crit}}$. In the following, we will discuss the two synchronization modes in turn.

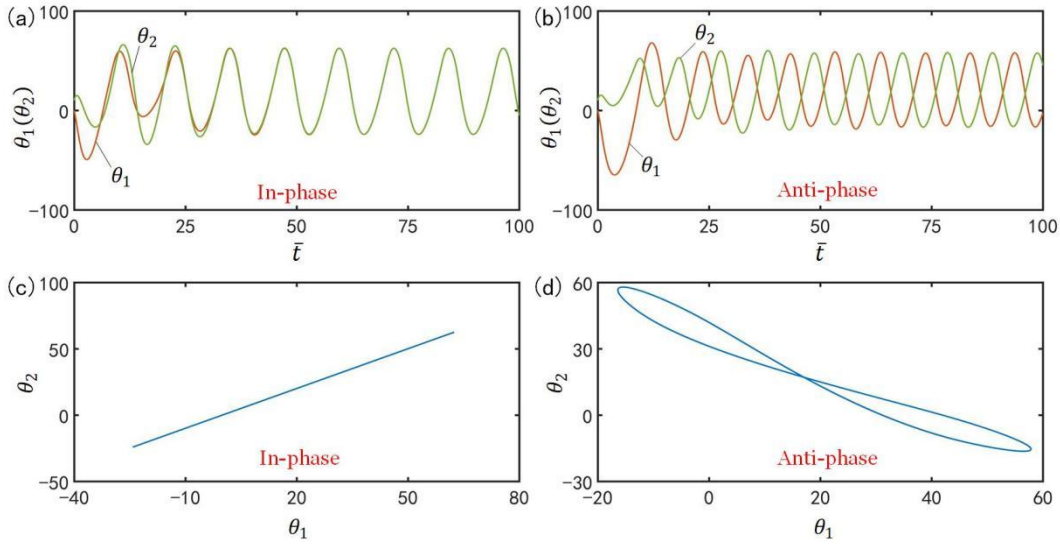

Fig. 2 Two kinds of synchronization modes of the light-powered self-excited LCE oscillators. The parameters are $\bar{I} = 0.25$, $C_0 = 0.4$, $\bar{g} = 9.8$, $k = 9.2$, $\bar{\beta} = 0.882$, $\dot{\theta}_1^0 = -0.33$, $\dot{\theta}_2^0 = 0.33$, $\theta_u = 45°$, $\theta_d = -80°$, $\theta_1^0 = 0°$ and $\theta_2^0 = 10°$. (a) and (b) correspond to two typical synchronization modes: in-phase mode for $\overline{\alpha} = 0.1$, and anti-phase mode for $\overline{\alpha} = 0.03$. (c) and (d) are domain of attraction of the two typical synchronization modes.

4 In-phase synchronization mode

4.1 Mechanisms of the self-excited oscillation in in-phase mode

To investigate the mechanism of the self-excited oscillation in in-phase mode of the two LCE oscillators under steady illumination, Fig. 3 presents time-histories of some key physical quantities of the in-phase mode in Figs. 2b and d. Fig. 3a plots the time histories of θ_1 or θ_2, which shows that the two LCE bars oscillate periodically in in-phase mode. Fig. 3b plots time histories of the number fractions of *cis*-isomers in the two LCE bars. The number fractions of *cis*-isomers increase in the light zone, while decrease in the dark zone. Therefore, the contraction strains in the two LCE bars increase in the light zone, while decrease in the dark zone, as shown in Fig. 3c, . In Fig. 3d, the moment of the torsion spring on the two bars is zero, because the angle

difference between the two bars in in-phase mode is zero. In Fig. 3e, the driving moments of the two oscillators also change periodically in in-phase mode.. Fig. 3f delineates the dependence of the driving moment on θ_1 or θ_2. In Fig, 3f, the area surrounded by the closed curve represents the net work done by the steady illumination during one cycle of the self-excited oscillation, which compensates for the energy dissipation caused by the damping to maintain the oscillation of the LCE oscillators.

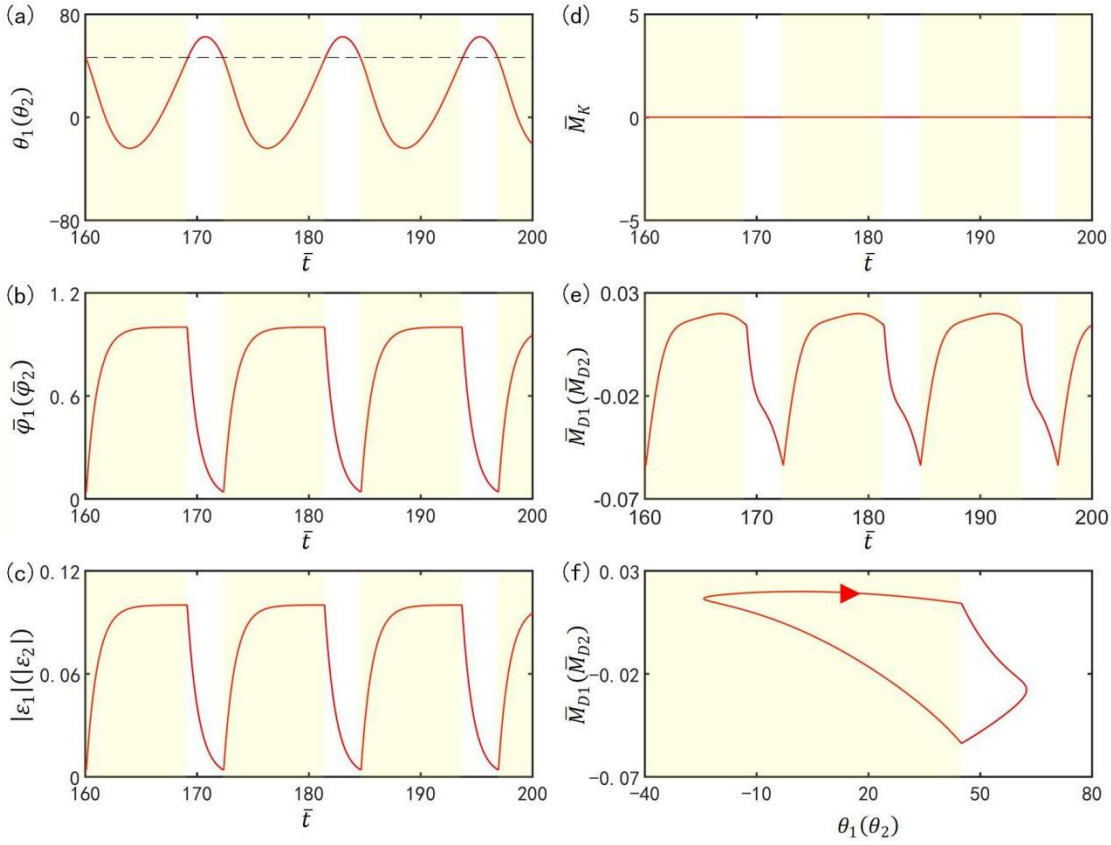

Fig. 3 Mechanism of the self-excited oscillation in in-phase mode. The parameters are $\bar{I}=0.25$, $C_0=0.4$, $\bar{g}=9.8$, $k=9.2$, $\bar{\beta}=0.882$, $\bar{\alpha}=0.1$, $\dot{\theta}_1^0=-0.33$, $\dot{\theta}_2^0=0.33$, $\theta_u=45°$, $\theta_d=-80°$, $\theta_1^0=0°$ and $\theta_2^0=10°$. (a) Time histories of θ_1 or θ_2. (b) Time histories of the number fractions of *cis*-isomers in the two LCE bars. (c) Time histories of contraction strains. (d) Time history of moment of the torsion spring . (e) Time histories of the driving moments. (f) The relationship between the driving moments and θ_1 or θ_2.

4.2 **Effect of the initial conditions on the in-phase mode**

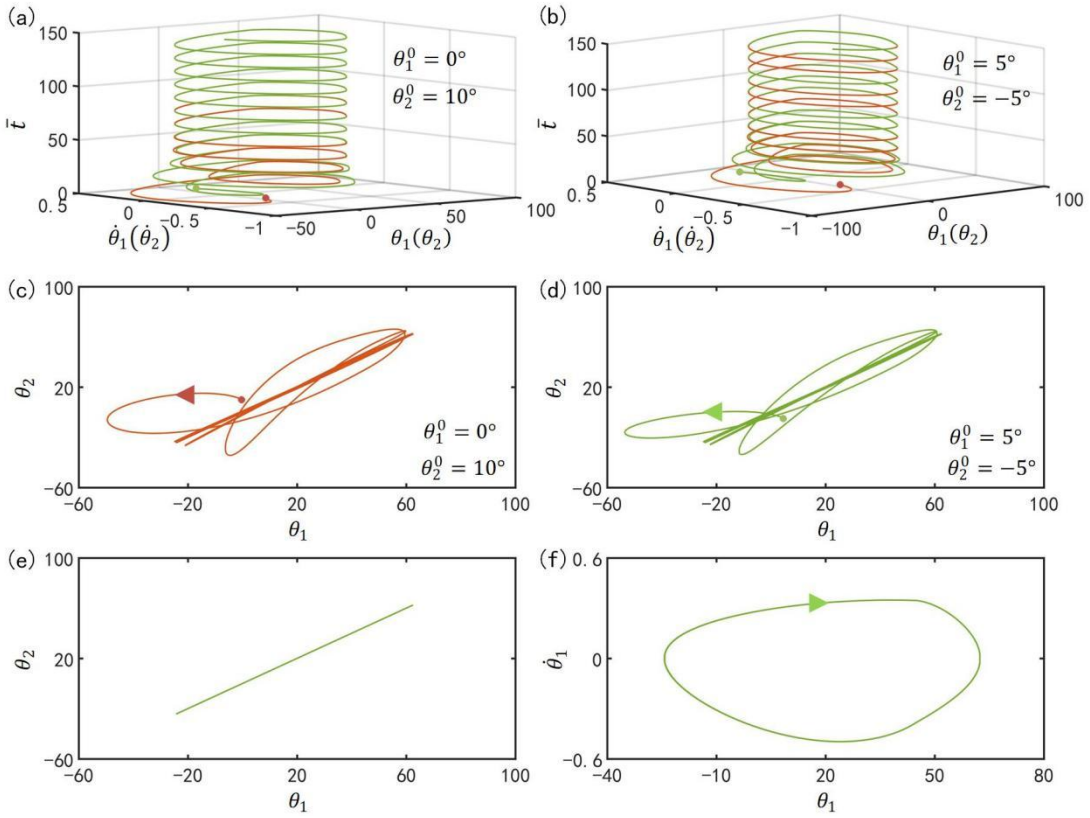

Fig. 4 Effect of initial conditions on the in-phase mode. The parameters are $\bar{I} = 0.25$, $C_0 = 0.4$, $\bar{g} = 9.8$, $k = 9.2$, $\bar{\beta} = 0.882$, $\bar{\alpha} = 0.1$, $\dot{\theta}_1^0 = -0.33$, $\dot{\theta}_2^0 = 0.33$, $\theta_u = 45°$ and $\theta_d = -80°$. (a) Time history for $\theta_1^0 = 0°$ and $\theta_2^0 = 10°$; (b) Time history for $\theta_1^0 = 5°$ and $\theta_2^0 = -5°$; (c) Phase diagrams for $\theta_1^0 = 0°$ and $\theta_2^0 = 10°$; (d) Phase diagrams for $\theta_1^0 = 5°$ and $\theta_2^0 = -5°$; (e) Domain of attraction of θ_1 and θ_2 for different initial conditions; (f) Limit cycles of θ_1 and $\dot{\theta}_1$ for different initial conditions.

Figs. 4a and b plot the time histories for two different initial conditions. In the computation, we set $\bar{I} = 0.25$, $C_0 = 0.4$, $\bar{g} = 9.8$, $k = 9.2$, $\bar{\beta} = 0.882$, $\bar{\alpha} = 0.1$, $\dot{\theta}_1^0 = -0.33$, $\dot{\theta}_2^0 = 0.33$, $\theta_u = 45°$ and $\theta_d = -80°$. In Figs. 4a and b, for the two different initial conditions, the two curves of the two LCE oscillators coincide after a period of time, which means that the two bars oscillate synchronously in in-phase mode. Figs. 4c and d plot the phase diagrams for the two initial conditions, in which θ_1 and θ_2 evolve from the initial disorder into a final attraction domain. Fig. 4e

further plots the domains of attraction of θ_1 and θ_2 for different initial conditions. The calculation shows that the two domains of attraction are the same. The results show that the initial condition has no effect on the synchronous mode.

Furthermore, Fig. 4f describes the limit cycles of θ_1 and $\dot{\theta}_1$ for different initial conditions. Similarly, the two limit cycles are also identical. This implies that the amplitude and frequency of the LCE oscillators are independent on the initial condition, which is further validated by more calculations. It is noted that the effect of initial condition on amplitude and frequency is similar to that of the single LCE oscillator [41].

4.3 **Effect of the spring constant on the in-phase mode**

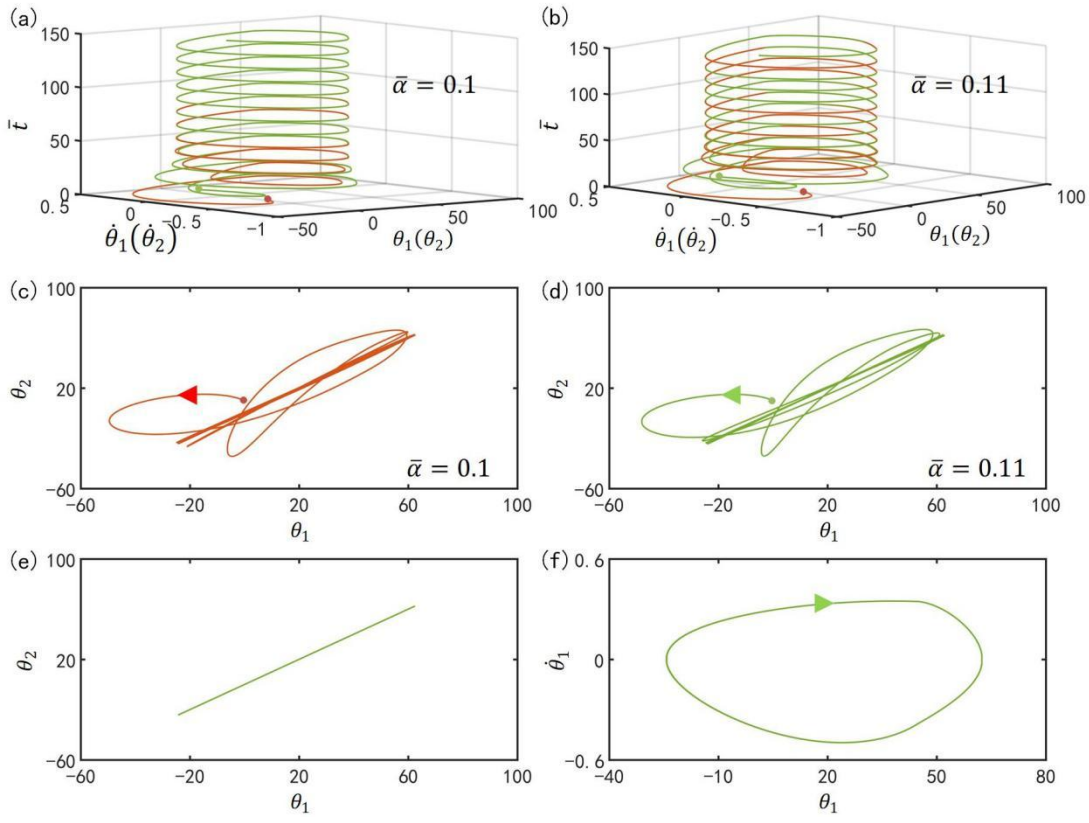

Fig. 5 Effect of spring constant on the in-phase mode. The parameters are $\bar{I} = 0.25$, $C_0 = 0.4$, $\bar{g} = 9.8$, $k = 9.2$, $\bar{\beta} = 0.882$, $\dot{\theta}_1^0 = -0.33$, $\dot{\theta}_2^0 = 0.33$, $\theta_u = 45°$, $\theta_d = -80°$, $\theta_1^0 = 0°$ and $\theta_2^0 = 10°$. (a) Time history for $\bar{\alpha} = 0.1$; (b) Time history for $\bar{\alpha} = 0.11$; (c) Phase diagrams for $\bar{\alpha} = 0.1$; (d) Phase diagrams for $\bar{\alpha} = 0.11$; (e) Domain of attraction of θ_1 and θ_2 for different spring constants; (f) Limit cycles of θ_1 and

$\dot{\theta}_1$ for different spring constants.

Figs. 5a and b plot the time histories of the two oscillators for different spring constants. In the computation, we set $\bar{I}=0.25$, $C_0=0.4$, $\bar{g}=9.8$, $k=9.2$, $\bar{\beta}=0.882$, $\dot{\theta}_1^0=-0.33$, $\dot{\theta}_2^0=0.33$, $\theta_u=45°$, $\theta_d=-80°$, $\theta_1^0=0°$ and $\theta_2^0=10°$. In Figs. 5a and b, for the two different spring constants, the two curves of the two LCE oscillators coincide after a period of time, which means that the two bars oscillate synchronously in in-phase mode. Figs. 5c and d plot the phase diagrams for the two spring constants, in which θ_1 and θ_2 evolve from the initial disorder into a final attraction domain. Fig. 5e further plots the domains of attraction of θ_1 and θ_2 for different spring constants. The calculation shows that the two domains of attraction are identical. The results show that the spring constant has no effect on the in-phase mode.

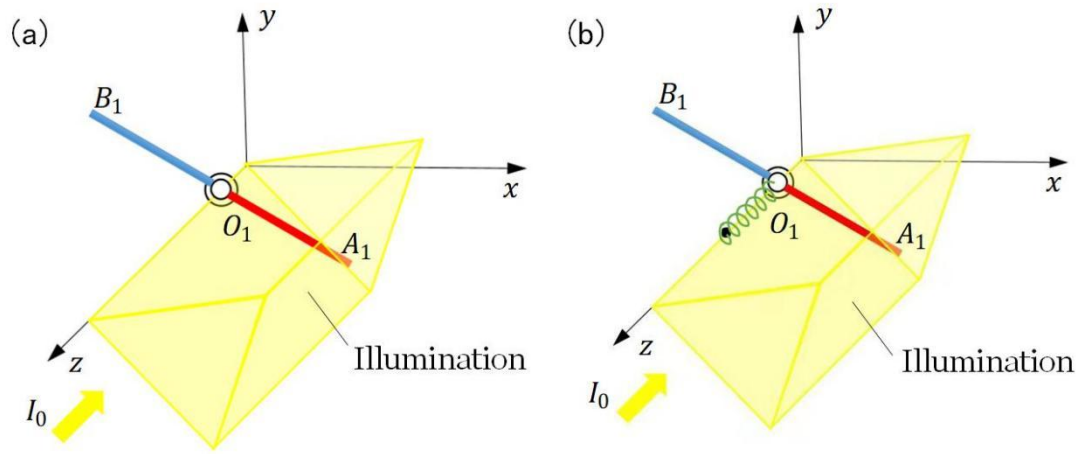

Fig. 6 Equivalent systems of (a) in-phase synchronization mode, and (b) anti-phase synchronization mode. In in-phase mode, the system is equivalent to the single oscillator. In anti-phase mode, the system is equivalent to the single oscillator with half-length torsion spring.

Furthermore, Fig. 5f describes the limit cycles of θ_1 and $\dot{\theta}_1$ for different spring constants. Similarly, the two limit cycles are also the same. This implies that the spring constant have no effect on the amplitude and frequency of the LCE oscillators. More calculations show that the influence of the spring constant is the same for

$\bar{\alpha} > \bar{\alpha}_{\text{crit}} = 0.075$. This is because that for $\bar{\alpha} > \bar{\alpha}_{\text{crit}}$, the LCE oscillators are in in-phase mode, and both the angle difference between two bars and the moment of spring are zero. Therefore, spring constant has no effect on the its amplitude and frequency. In in-phase mode, the system is equivalent to the single oscillator, as shown in Fig. 6a.

5 Anti-phase synchronization mode

5.1 Mechanisms of the self-excited oscillation in anti-phase mode

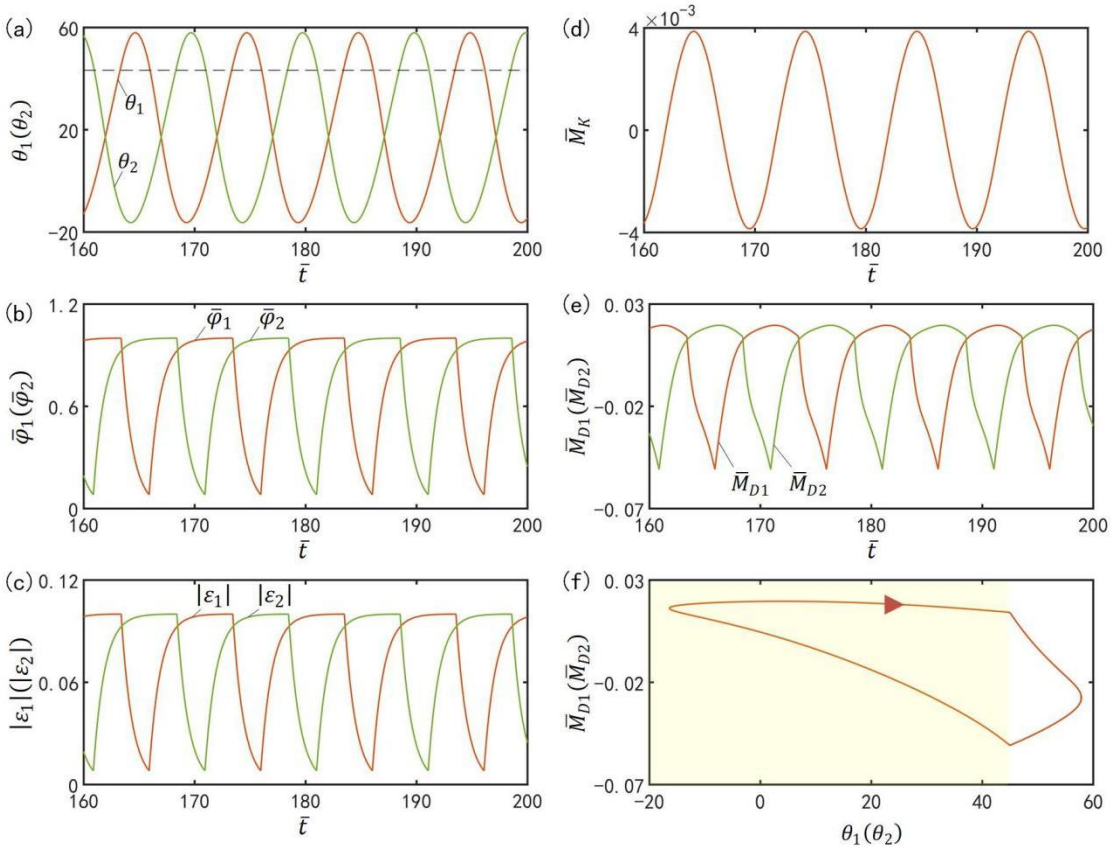

Fig. 7 Mechanism of the self-excited oscillation in anti-phase mode. The parameters are $\bar{I} = 0.25$, $C_0 = 0.4$, $\bar{g} = 9.8$, $k = 9.2$, $\bar{\beta} = 0.882$, $\bar{\alpha} = 0.03$, $\dot{\theta}_1^0 = -0.33$, $\dot{\theta}_2^0 = 0.33$, $\theta_u = 45°$, $\theta_d = -80°$, $\theta_1^0 = 0°$ and $\theta_2^0 = 10°$. (a) Time histories of θ_1 or θ_2. (b) Time histories of the number fractions of *cis*-isomers in the two LCE bars. (c) Time histories of contraction strains. (d) Time history of moment of the torsion spring. (e) Time histories of the driving moments. (f) The relationship between the driving moments and θ_1 or θ_2.

To investigate the mechanism of the self-excited oscillation in anti-phase mode

of the two LCE oscillators under steady illumination, Fig. 7 presents time-histories of some key physical quantities of the anti-phase mode in Figs. 2a and 2c. Fig. 7a plots the time histories of θ_1 and θ_2, which shows that the two LCE bars oscillate periodically in anti-phase mode. Fig. 7b plots time histories of the number fractions of *cis*-isomers in the two LCE bars. Similarly, the number fractions of *cis*-isomers also increase in the light zone, while decrease in the dark zone. Therefore, the contraction strains in the two LCE bars increase in the light zone, while decrease in the dark zone, as shown in Fig. 7c. In Fig. 7d, the moment of the torsion spring on the two bars changes periodically, because the angle difference between the two bars in anti-phase mode varies periodically. In Fig. 7e, the driving moments of the two oscillators in anti-phase mode also fluctuates periodically. Fig. 7f delineates the dependence of the driving moment on θ_1 or θ_2. In Fig, 7f, the area surrounded by the closed curve represents the net work done by the steady illumination during one cycle of the self-excited oscillation, which compensates for the energy loss caused by the damping to maintain the oscillation of the LCE oscillators.

5.2 Effect of initial conditions on the anti-phase mode

Figs. 8a and b plot the time histories for two different initial conditions. In the computation, we set $\bar{I}=0.25$, $C_0=0.4$, $\bar{g}=9.8$, $k=9.2$, $\bar{\beta}=0.882$, $\bar{\alpha}=0.03$, $\dot{\theta}_1^0=-0.33$, $\dot{\theta}_2^0=0.33$, $\theta_u=45°$ and $\theta_d=-80°$. In Figs. 8a and b, for two different initial conditions, the self-excited oscillations of the two LCE oscillators have a phase difference of half a cycle after a period of time, which means that the two bars oscillate synchronously in anti-phase mode. Figs. 8c and d plot the phase diagrams for the two initial conditions, in which θ_1 and θ_2 evolve from the initial disorder into a final attraction domain. Fig. 8e further plots the domains of attraction of θ_1 and θ_2 for different initial conditions. The calculation shows that the two domains of attraction are the same. The results also show that the initial condition has no effect on the synchronous mode.

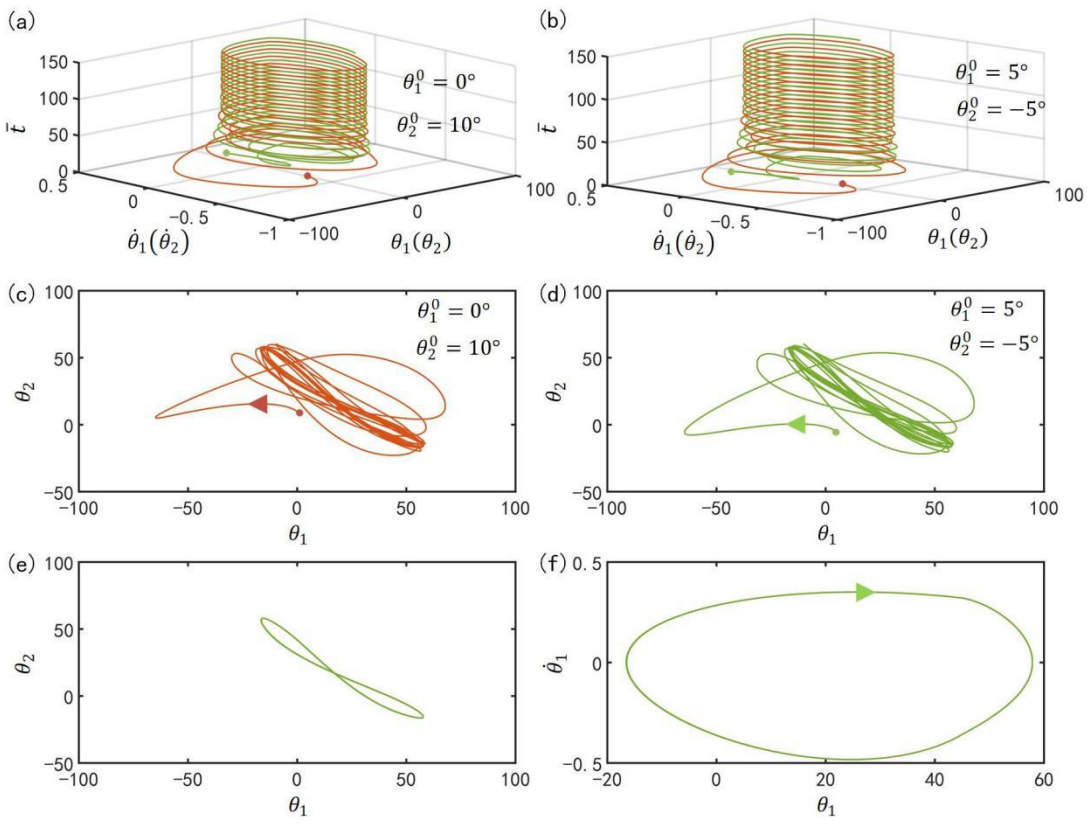

Fig. 8 Effect of initial conditions on the anti-phase mode. The parameters are $\bar{I} = 0.25$, $C_0 = 0.4$, $\overline{g} = 9.8$, $k = 9.2$, $\overline{\beta} = 0.882$, $\overline{\alpha} = 0.03$, $\dot{\theta}_1^0 = -0.33$, $\dot{\theta}_2^0 = 0.33$, $\theta_u = 45°$ and $\theta_d = -80°$. (a) Time history for $\theta_1^0 = 0°$ and $\theta_2^0 = 10°$; (b) Time history for $\theta_1^0 = 5°$ and $\theta_2^0 = -5°$; (c) Phase diagrams for $\theta_1^0 = 0°$ and $\theta_2^0 = 10°$; (d) Phase diagrams for $\theta_1^0 = 5°$ and $\theta_2^0 = -5°$; (e) Domain of attraction of θ_1 and θ_2 for different initial conditions; (f) Limit cycles of θ_1 and $\dot{\theta}_1$ for different initial conditions.

Furthermore, Fig. 8f describes the limit cycles of θ_1 and $\dot{\theta}_1$ for different initial conditions. Similarly, the two limit cycles are also identical. This implies that the amplitude and frequency of the LCE oscillators are independent on the initial condition. More calculations also show that the influence of initial conditions is the same. It is noted that the effect of initial condition on amplitude and frequency of the anti-phase mode is similar to that of the single LCE oscillator [41].

5.3 Effect of the spring constant on the anti-phase mode

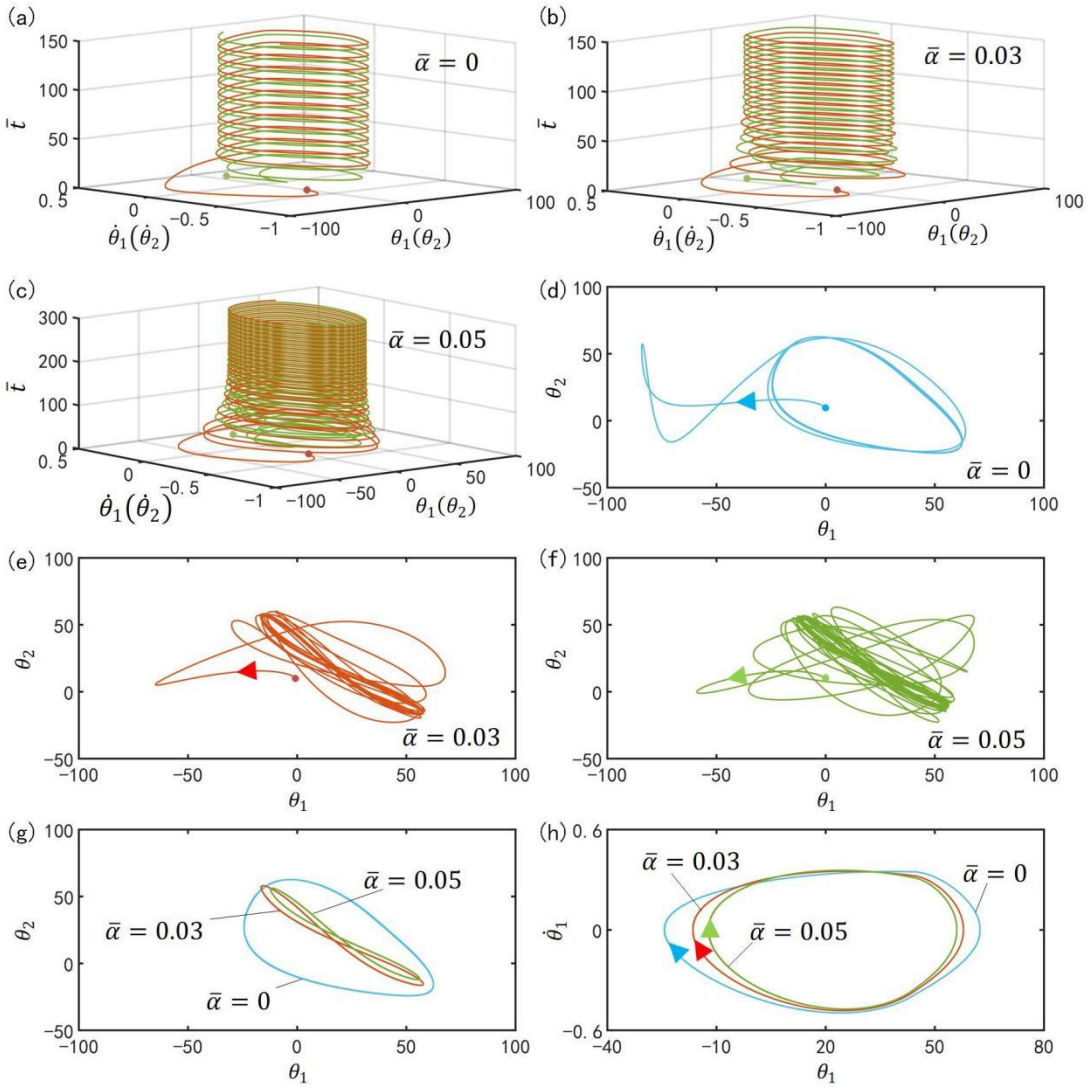

Fig. 9 Effect of spring constant on the anti-phase mode. The parameters are $\bar{I} = 0.25$, $C_0 = 0.4$, $\bar{g} = 9.8$, $k = 9.2$, $\bar{\beta} = 0.882$, $\dot{\theta}_1^0 = -0.33$, $\dot{\theta}_2^0 = 0.33$, $\theta_u = 45°$, $\theta_d = -80°$, $\theta_1^0 = 0°$ and $\theta_2^0 = 10°$. (a) Time history for $\bar{\alpha} = 0$; (b) Time history for $\bar{\alpha} = 0.03$; (c) Time history for $\bar{\alpha} = 0.05$; (d) Phase diagrams for $\bar{\alpha} = 0$; (e) Phase diagrams for $\bar{\alpha} = 0.03$; (f) Phase diagrams for $\bar{\alpha} = 0.05$; (g) Domain of attraction of θ_1 and θ_2 for different spring constants; (h) Limit cycles of θ_1 and $\dot{\theta}_1$ for different spring constants.

Figs. 9a-c plot the time history for different spring constants. In the computation, we set $\bar{I} = 0.25$, $C_0 = 0.4$, $\bar{g} = 9.8$, $k = 9.2$, $\bar{\beta} = 0.882$, $\dot{\theta}_1^0 = -0.33$, $\dot{\theta}_2^0 = 0.33$, $\theta_u = 45°$, $\theta_d = -80°$, $\theta_1^0 = 0°$ and $\theta_2^0 = 10°$. For $\bar{\alpha} = 0$, the phase difference between

the two bars after a period of time is a constant value that is generally not $180°$ or $0°$, as shown in Fig. 9a. Fig. 9d plots the phase diagrams for $\overline{\alpha}=0$, in which θ_1 and θ_2 evolve from the initial disorder into a final attraction domain. The domains of attraction of θ_1 and θ_2 and limit cycles of θ_1 and $\dot{\theta}_1$ are further plotted in Figs. 9g and h, respectively. Through calculation, we find that for $\overline{\alpha}=0$, the final phase difference of two bars depends on initial conditions, while the limit cycles are independent on the initial conditions. It can be understood that for $\overline{\alpha}=0$, the system is equivalent to the single oscillator [41], and the phase difference is determined by their independent self-excited oscillations.

In Figs. 9b and c, for $\overline{\alpha}=0.03$ and $\overline{\alpha}=0.05$, the self-excited oscillations of the two LCE oscillators have a phase difference of half a cycle after a period of time, which means that the two bars oscillate synchronously in anti-phase mode. Figs. 9e and f plot the phase diagrams for $\overline{\alpha}=0.03$ and $\overline{\alpha}=0.05$, in which θ_1 and θ_2 evolve from the initial disorder into a final attraction domain. Furthermore, Fig. 9g and h plot the domains of attraction of θ_1 and θ_2 and the limit cycles of θ_1 and $\dot{\theta}_1$. Obviously, the domains of attraction and the limit cycles are also different. It can be seen that its amplitude decreases with the increase of the spring constant. Careful calculation shows that the period also decreases with the increase of the spring constant. Actually, the system in anti-phase mode for $\overline{\alpha}<\overline{\alpha}_{\text{crit}}$ is equivalent to single self-excited oscillator constrained by a fixed torsion spring with half original length, as shown in Fig. 6b. The greater the spring constant, the smaller the amplitude and the period. This result is consistent with the physical intuition [44].

6 Conclusions

Based on self-excited oscillator composed of LCE bars, the synchronization of two identical self-excited oscillators is studied in this paper. Combing dynamic LCE model, a theoretical model for the self-excited motion of the two self-excited oscillators connected by a torsion spring, and synchronization of the self-excited

motion is numerically calculated by *MATLAB* software. It is found that self-excited oscillation of the system has two synchronization modes: in-phase mode and anti-phase mode. By plotting the time histories of various quantities, we elucidate the mechanism of self-excited oscillation and the two synchronization modes. Furthermore, the effects of initial conditions and interaction on the two synchronization modes of the self-excited oscillation are investigated systematically, by plotting their contractors of the system. For strong interactions, the system always develops into in-phase synchronization mode, and both its amplitude and period are independent on the interaction. In this case, the system is equivalent to two identical self-excited oscillators without interaction. For weak interaction, the system will evolve into anti-phase synchronization mode, and its amplitude decreases with the increase of the interaction. In this case, it is equivalent to single self-excited oscillator constrained by fixed torsion spring with half original length. Meanwhile, the initial condition generally does not affect the synchronization mode and its amplitude. This study will deepen people's understanding of interaction and synchronization of self-excited motions, and provide promising applications in energy acquisition, power generation, monitoring, soft robot, medical equipment and micro nano devices.

Declarations

Data Availability Statements

All data generated or analysed during this study are included in this published article.

Acknowledgements

This work is supported by Key Project of Natural Science Research of Universities in Anhui under Grant Nos. KJ2020A0449 and KJ2020A0452.

Ethical standards

The authors ensure the compliance with ethical standards for this work.

Conflict of interest

The authors declare that they have no conflict of interest.

References

1. Li, M.H., Keller, P., Li, B., Wang, X., Brunet, M.: Light-driven side-on nematic elastomer actuators. Adv. Mater. **15**, 569–572 (2003). http://doi.org/10.1002/adma.200304552

2. Wang, X., Tan, C.F., Chan, K.H., Lu, X., Zhu, L., Kim, S., Ho, G.W.: In-built thermo-mechanical cooperative feedback mechanism for self-propelled multimodal locomotion and electricity generation. Nat. Commun. **9**, 3438 (2018). https://doi.org/10.1038/s41467-018-06011-9

3. Nocentini, S., Parmeggiani, C., Martella, D., Wiersma, D.S.: Optically driven soft micro robotics. Adv. Opt. Mater. **6**, 1800207 (2018). https://doi.org/10.1002/adom.201800207

4. Ge, F., Yang, R., Tong, X., Camerel, F., Zhao, Y.: A multifunctional dyedoped liquid crystal polymer actuator: light-guided transportation, turning in locomotion, and autonomous motion. Angew. Chem. Int. Ed. **57**, 11758–11763 (2018). https://doi.org/10.1002/ange.201807495

5. Preston, D.J., Jiang, H.J., Sanchez, V., Rothemund, P., Rawson, J., Nemitz, M.P., Lee, W., Suo, Z., Walsh, C.J., Whitesides, G.M.: A soft ring oscillator. Sci. Robot. **4**, eaaw5496 (2019). https://doi.org/10.1126/scirobotics.aaw5496

6. Zeng, H., Lahikainen, M., Liu, L., Ahmed, Z., Wani, O.M., Wang, M., Priimagi, A.: Light-fuelled freestyle self-oscillators. Nat. Commun. **10**(1), 1-9 (2019). https://doi.org/10.1038/s41467-019-13077-6

7. Kinoshita, S.: Introduction to nonequilibrium phenomena, pattern formations and oscillatory phenomena. 1–59 (2013). https://doi.org/10.1016/B978-0-12-397014-5.00001-8

8. Chakrabarti, A., Choi, G.P.T., Mahadevan, L.: Self-excited motions of volatile drops on swellable sheets. Phys. Rev. Lett. **124**(25), 258002 (2020). https://doi.org/10.1103/PhysRevLett.124.258002

9. Kriegman, S., Blackiston, D., Levin, M., Bongard, J.: A scalable pipeline for

designing reconfigurable organisms. P. Natl. Acad. Sci.USA. **117**(4), 1853-1859 (2020).
https://doi.org/ 10.1073/pnas.1910837117
10. Hu, W., Lum, G.Z., Mastrangeli, M., Sitti, M.: Small-scale soft-bodied robot with multimodal locomotion. Nat. **554**(7690), 81-85 (2018).
https://doi.org/ 10.1038/nature25443
11. Huang, H., Aida, T.: Towards molecular motors in unison. Nat. Nanotechnol. **14**(5), 407-407 (2019).
https://doi.org/ 10.1038/s41565-019-0414-1
12. Sangwan, V., Taneja, A., Mukherjee, S.: Design of a robust self-excited biped walking mechanism. Mech. Mach. Theory. **39**(12), 1385-1397 (2004).
https://doi.org/ 10.1016/j.mechmachtheory.2004.05.023
13. Chatterjee, S.: Self-excited oscillation under nonlinear feedback with time-delay. J. Sound Vib. **330**(9), 1860-1876 (2011).
https://doi.org/ 10.1016/j.jsv.2010.11.005
14. Lu, X., Zhang, H., Fei, G., Yu, B., Tong, X., Xia, H., Zhao, Y.: Liquid-crystalline dynamic networks doped with gold nanorods showing enhanced photocontrol of actuation. Adv. Mater. **30**(14), 1706597 (2018).
https://doi.org/ 10.1002/adma.201706597
15. Cheng, Y., Lu, H., Lee, X., Zeng, H., Priimagi, A.: Kirigami-based light-induced shape-morphing and locomotion. Adv. Mater. **32**(7), 1906233 (2019).
https://doi.org/ 10.1002/adma.201906233
16. Vantomme, G., Gelebart, A.H., Broer, D.J., Meijer, E.W.: A four-blade light-driven plastic mill based on hydrazone liquid-crystal networks. Tetrahedron. **73**(33), 4963-4967 (2017).
https://doi.org/ 10.1016/j.tet.2017.06.041
17. Lahikainen, M., Zeng, H., Priimagi, A.: Reconfigurable photoactuator through synergistic use of photochemical and photothermal effects. Nat. Commun. **9,** 4148 (2018).
https://doi.org/ 10.1038/s41467-018-06647-7

18. Gelebart A.H., Mulder D.J., Varga M., Konya A., Vantomme, G., Meijer, E.W., Selinger, R.S., Broer, D.J.: Making waves in a photoactive polymer film. Nat. **546**(7660), 632-636 (2017).
https://doi.org/ 10.1038/nature22987
19. Boissonade, J., Kepper, P. De.: Multiple types of spatio-temporal oscillations induced by differential diffusion in the Landolt reaction. Phys. Chem. Chem. Phys. **13**, 4132–4137 (2011).
https://doi.org/10.1039/c0cp01653e
20. Li, K., Wu, P.Y., Cai, S.Q.: Chemomechanical oscillations in a responsive gel induced by an autocatalytic reaction. J. Appl. Phys. **116**(4), 043523 (2014).
https://doi.org/ 10.1063/1.4891520
21. Camacho, L.M., Finkelmann, H., Palffy, M.P., Shelley, M.: Fast liquid-crystal elastomer swims into the dark. Nat. Mater. **3**(5), 307-310 (2004).
https://doi.org/ 10.1038/nmat1118
22. Lu, X., Guo, S., Tong, X., Xia, H., Zhao, Y.: Tunable photo controlled motions using stored strain energy in malleable azobenzene liquid crystalline polymer actuators. Adv. Mater. **29**(28), 1606467 (2017).
https://doi.org/10.1002/adma.201606467
23. White, T., Tabiryan, N., Serak, S., Hrozhyk, U., Tondiglia, V., Koerner, H.: Vaia, R.; Bunning, T.; A high frequency photodriven polymer oscillator. Soft Matter. **4**(9), 1796-1798 (2008).
https://doi.org/ 10.1039/b805434g
24. Lee M.K., Smith, M., Koerner, H., Tabiryan, N., Vaia, R., Bunning, T., White, T.: Photodriven, flexural–torsional oscillation of glassy azobenzene liquid crystal polymer networks. Adv. Funct. Mater. **21**(15), 2913-2918 (2011).
https://doi.org/ 10.1002/adfm.201100333
25. Yamada, M., Kondo, M., Mamiya, J., Yu, Y., Kinoshita, M., Barrett, C., Ikeda, T.: Photomobile polymer materials: towards light - driven plasticmotors. Angew, Chem. Int, Edit. **47**(27), 4986-4988 (2008).
https://doi.org/ 10.1002/anie.200800760

521 26. Gelebart, H.A., Vantomme, G., Meijer, E.W., Broer, D.: Mastering the
522 photothermal effect in liquid crystal networks: a general approach for self - sustained
523 mechanical oscillators. Adv. Mater. **29**(18), 1606712 (2017).
524 https://doi.org/ 10.1002/adma.201606712
525 27. Vantomme, G., Gelebart, H.A., Broer, J.D., Meijer, E.W.: Self - sustained
526 actuation from heat dissipationin liquid crystal polymer networks. J. Polym. Sci. Pol.
527 Chem. **56**(13), 1331-1336 (2018).
528 https://doi.org/ 10.1002/pola.29032
529 28. Ahn, C., Li, K., Cai, S.: Light or thermally powered autonomous rolling of an
530 elastomer rod. Acs. Appl Mater. Inter. **10**(30), 25689-25696 (2018).
531 https://doi.org/ 10.1021/acsami.8b07563
532 29. Yang, L., Chang, L., Hu, Y., Huang, M., Ji, Q., Lu, P., Liu, J., Chen, W., Wu, Y.:
533 An autonomous soft actuator with light - driven self - sustained wavelike oscillation
534 for phototactic self - locomotion and power generation. Adv. Funct. Mater. 1908842
535 (2020).
536 https://doi.org/ 10.1002/adfm.202070095
537 30. Kageyama, Y., Ikegami, T., Satonaga, S., Obara, K., Sato, H., Takeda, S.:
538 Light - driven flipping of azobenzene assemblies-sparse crystal structures and
539 responsive behavior to polarized light, Chemistry–A European Journal. 2000701
540 (2020).
541 https://doi.org/10.1002/chem.202000701
542 31. Zhao, D., Liu, Y.: A prototype for light-electric harvester based on light sensitive
543 liquid crystal elastomer cantilever. Energy. **198**, 117351 (2020).
544 https://doi.org/ 10.1016/j.energy.2020.117351
545 32. Kuenstler, A., Chen, Y., Bui, P., Kim, H., DeSimone, A., Jin, L., Hayward, R.:
546 Blueprinting photothermal shape-morphing of liquid crystal elastomers. Adv. Mater.
547 2000609, 1-9 (2020).
548 https://doi.org/ 10.1002/adma.202000609
549 33. Strogatz, S.: Synchronization: A Universal Concept in Nonlinear Science. Physics.
550 Today. **56**(1), 47-47 (2003).

https://doi.org/10.1063/1.1554136

34. Vicsek, T. Zafeiris, A.: Collective motion. Phys. Reports. **517**(3-4), 71-140 (2012).

https://doi.org/10.1016/j.physrep.2012.03.004

35. Boccaletti, S.: The Synchronized Dynamics of Complex Systems. Monograph. **6**, 1-239 (2008).

https://doi.org/10.1016/S1574-6917(07)06001-1

36. O'Keeffe, K.P. Hong, H. Strogatz, S.H.: Oscillators that sync and swarm. Nat Communications. **8**(1), 1504 (2017).

https://doi.org/10.1038/s41467-017-01190-3

37. Bennett, M. Schatz, M.F. Rockwood,H.: Huygens's clocks. P Roy Soc A-math Phy. **458**(2019), 563-579 (2002).

https://doi.org/10.1098/rspa.2001.0888

38. Ramirez, J.P. Olvera, L.A. Nijmeijer, H.: The sympathy of two pendulum clocks: beyond Huygens' observations. Scientific Reports. **6**, 23580 (2016).

https://doi.org/10.1038/srep23580

39. Ikeguchi, T. Shimada, Y.: Analysis of Synchronization of Mechanical Metronomes. 2019.

https://doi.org/10.1007/978-3-030-10892-2

40. Ghislaine, V. Lars, C.M.E. Anne, H.G.: Coupled liquid crystalline oscillators in Huygens' synchrony.

https://doi.org/10.1038/s41563-021-00931-6

41. Cheng, Q. Liang, X. Li, K.: Light-powered self-excited motion of a liquid crystal elastomer rotator. Nonlinear. Dyn.1-13.(2021).

https://doi.org/10.1007/s11071-021-06250-4

42. Warner, M. Terentjev, E.M.: Liquid crystal elastomers. Oxford University Press. (2007).

43. Yu, Y. Nakano, M. Ikeda, P. T.: Directed bending of a polymer film by light-miniaturizing a simple photomechanical system could expand its range of applications. Nature. **425**, 145 (2003).

https://doi.org/10.1038/425145a

581 44. Bishop, R.E.D. Daniel, C.J.: The mechanics of vibration. Cambridge University
582 Press. (2011).
583

Figures

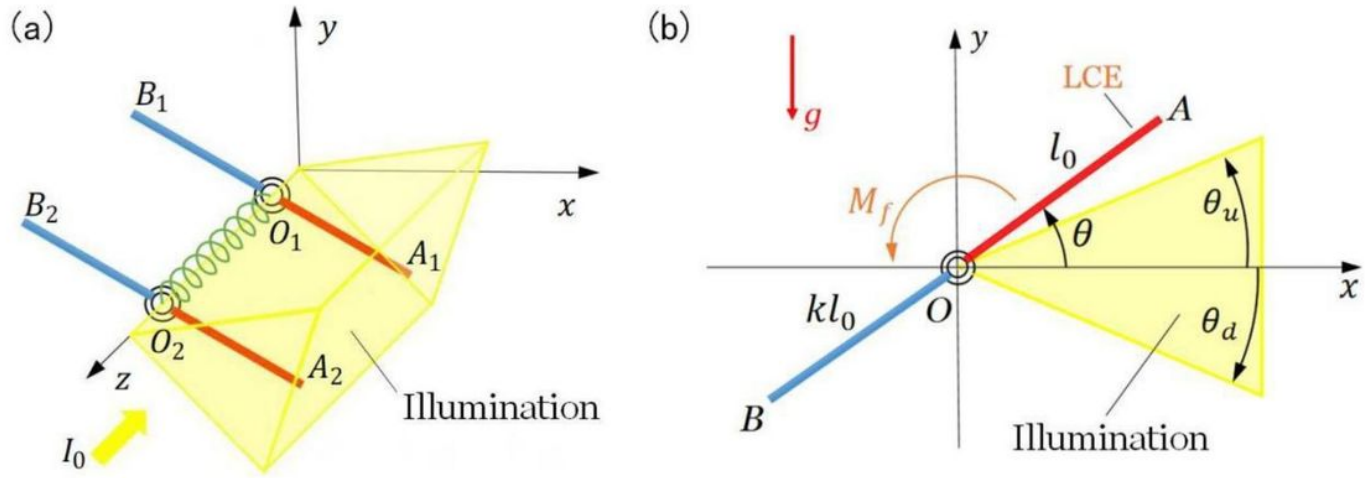

Figure 1

Please see the Manuscript PDF file for the complete figure caption

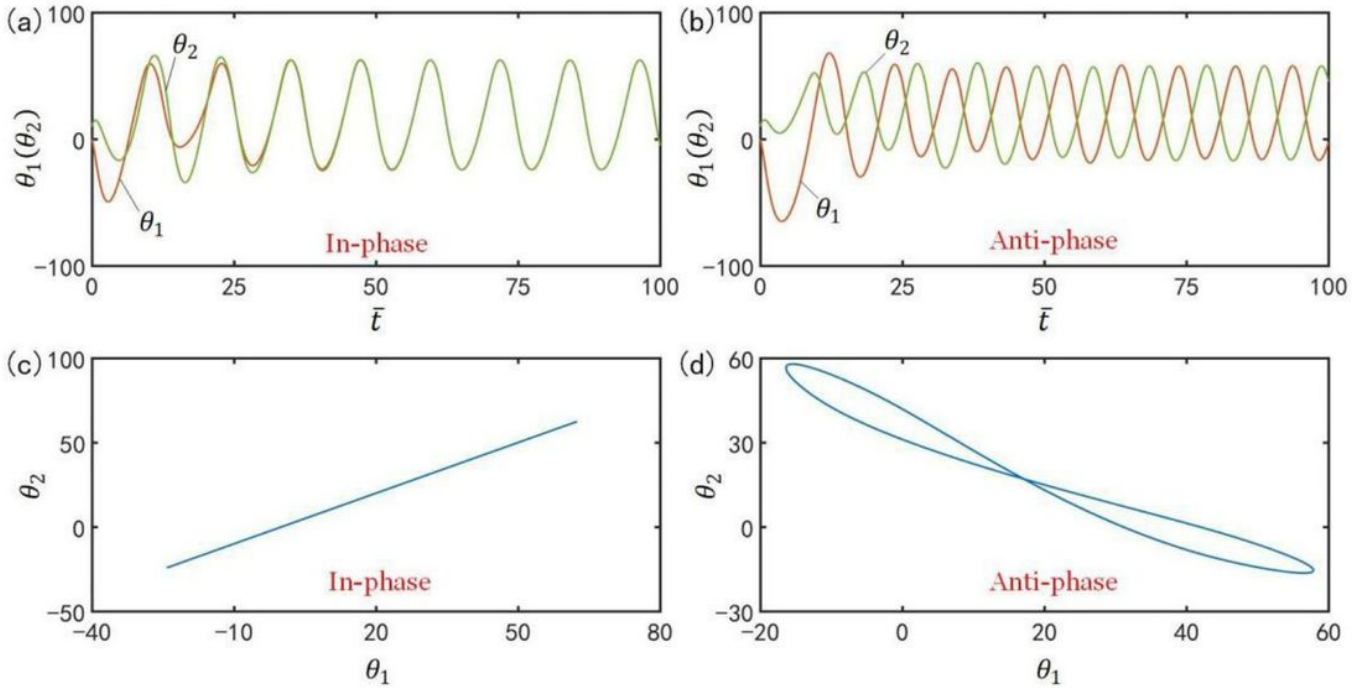

Figure 2

Please see the Manuscript PDF file for the complete figure caption

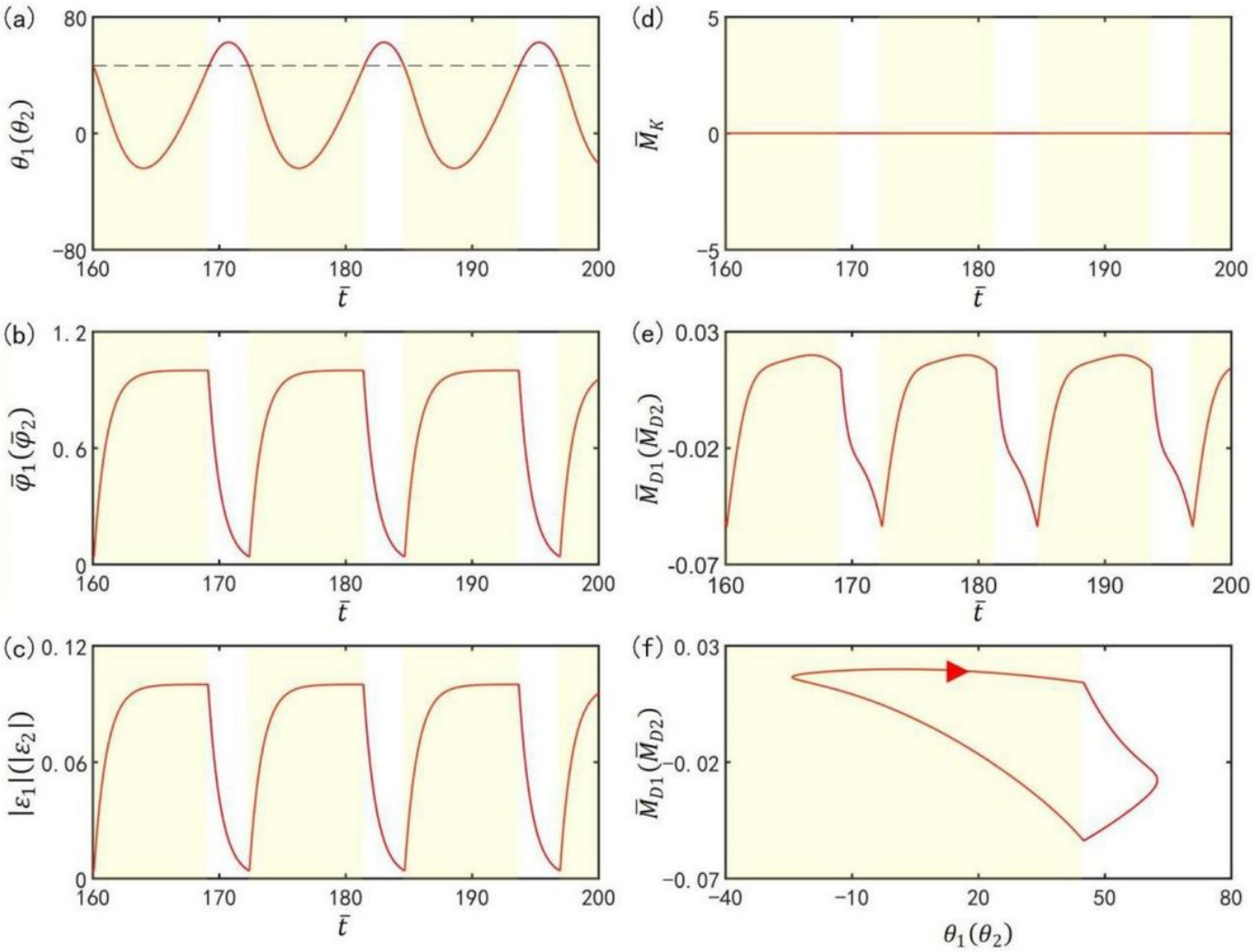

Figure 3

Please see the Manuscript PDF file for the complete figure caption

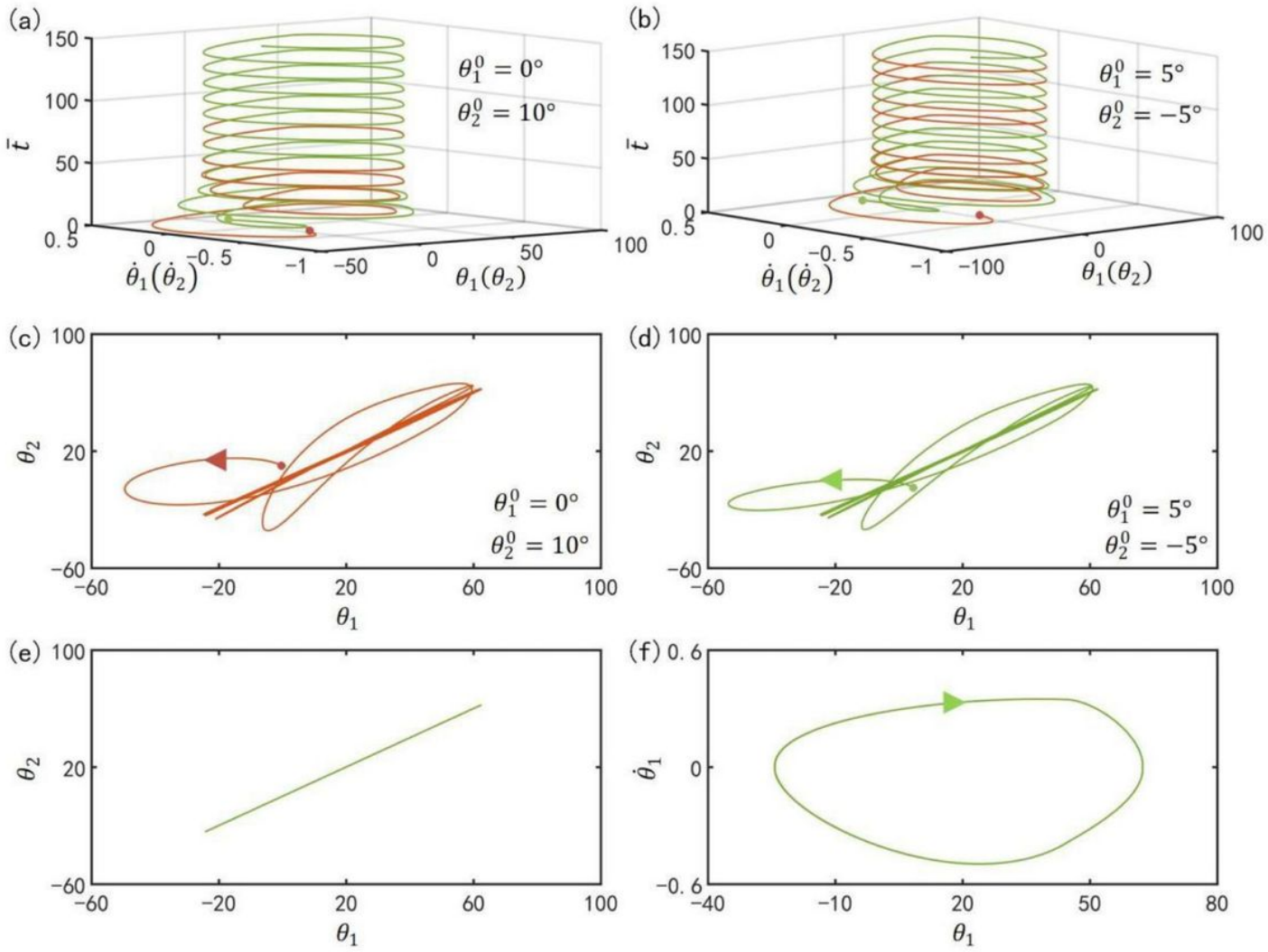

Figure 4

Please see the Manuscript PDF file for the complete figure caption

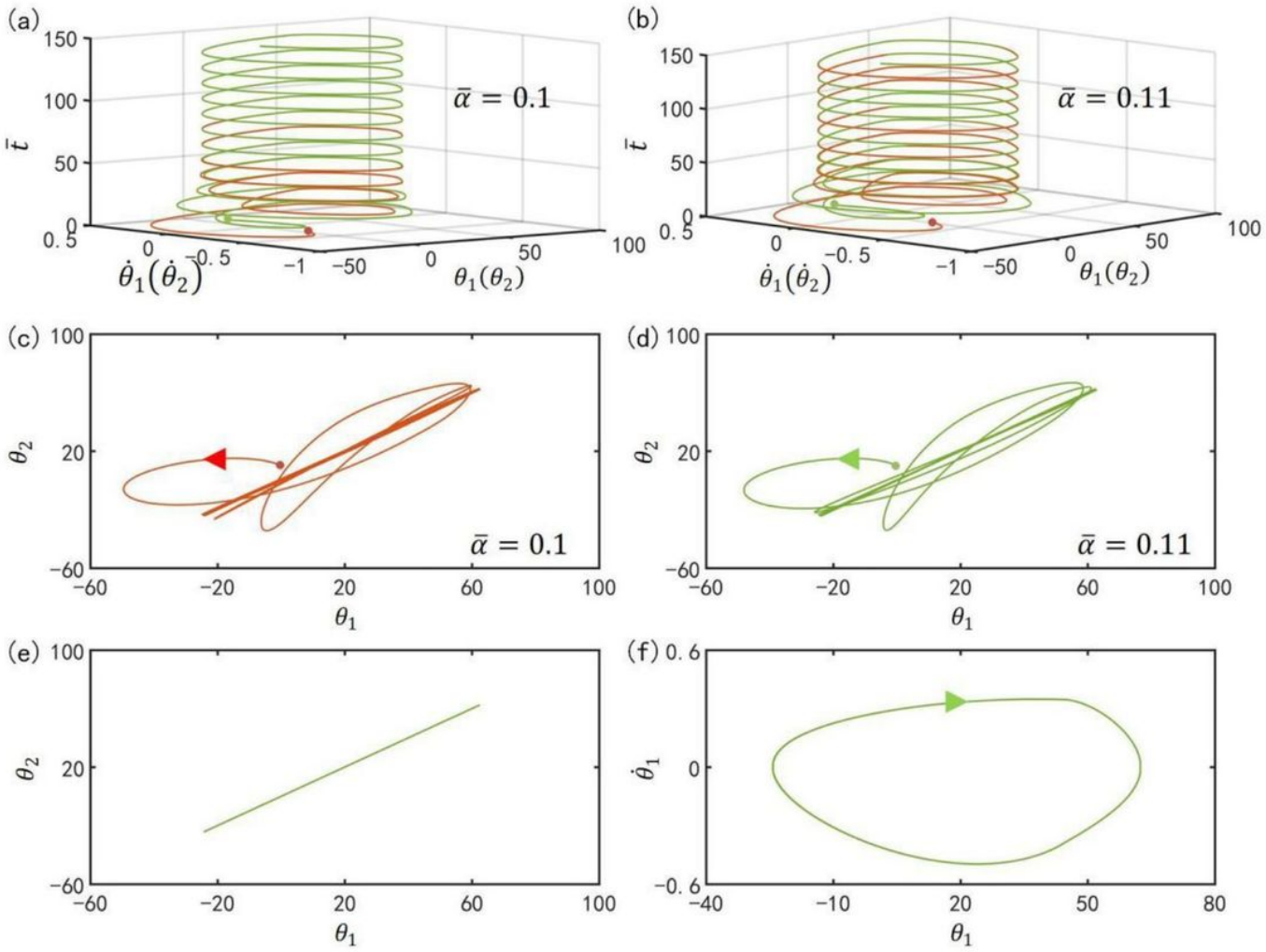

Figure 5

Please see the Manuscript PDF file for the complete figure caption

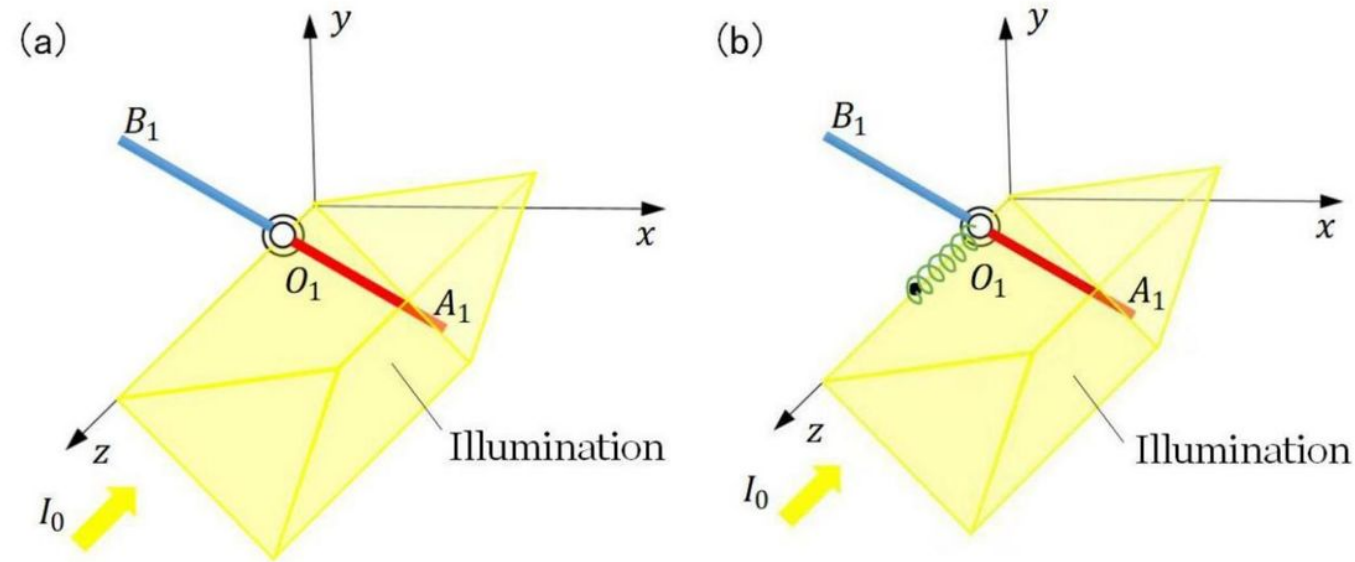

Figure 6

Please see the Manuscript PDF file for the complete figure caption

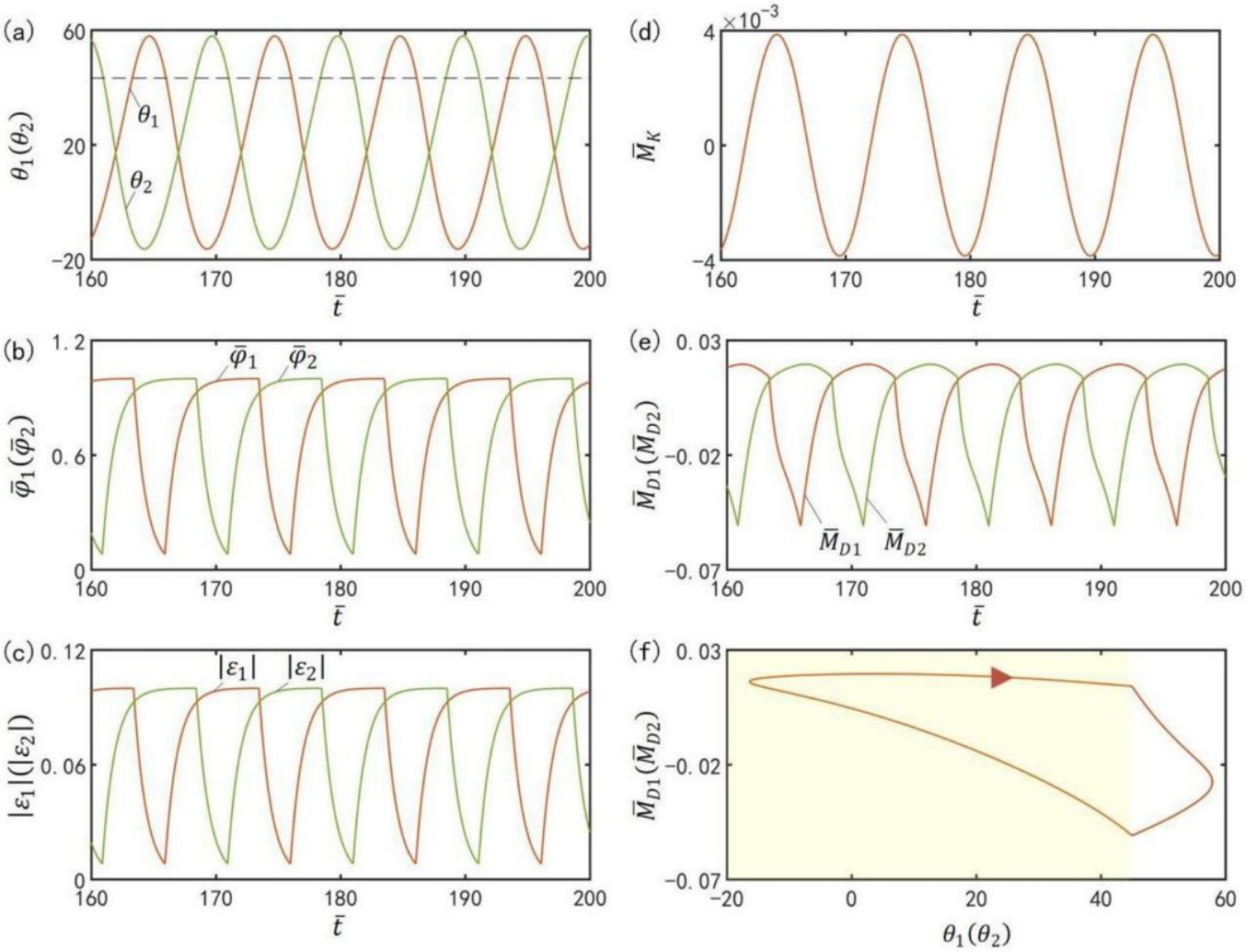

Figure 7

Please see the Manuscript PDF file for the complete figure caption

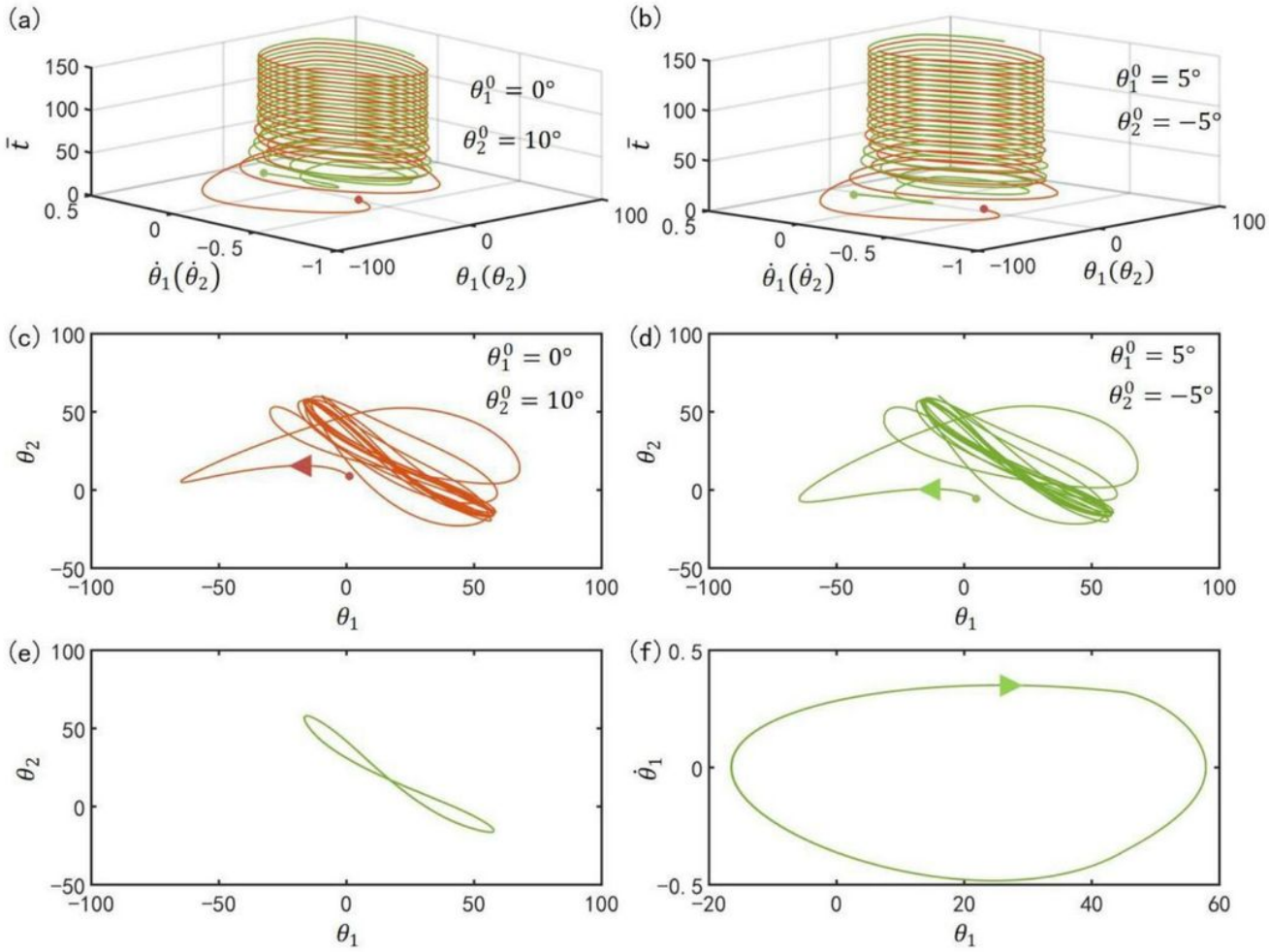

Figure 8

Please see the Manuscript PDF file for the complete figure caption

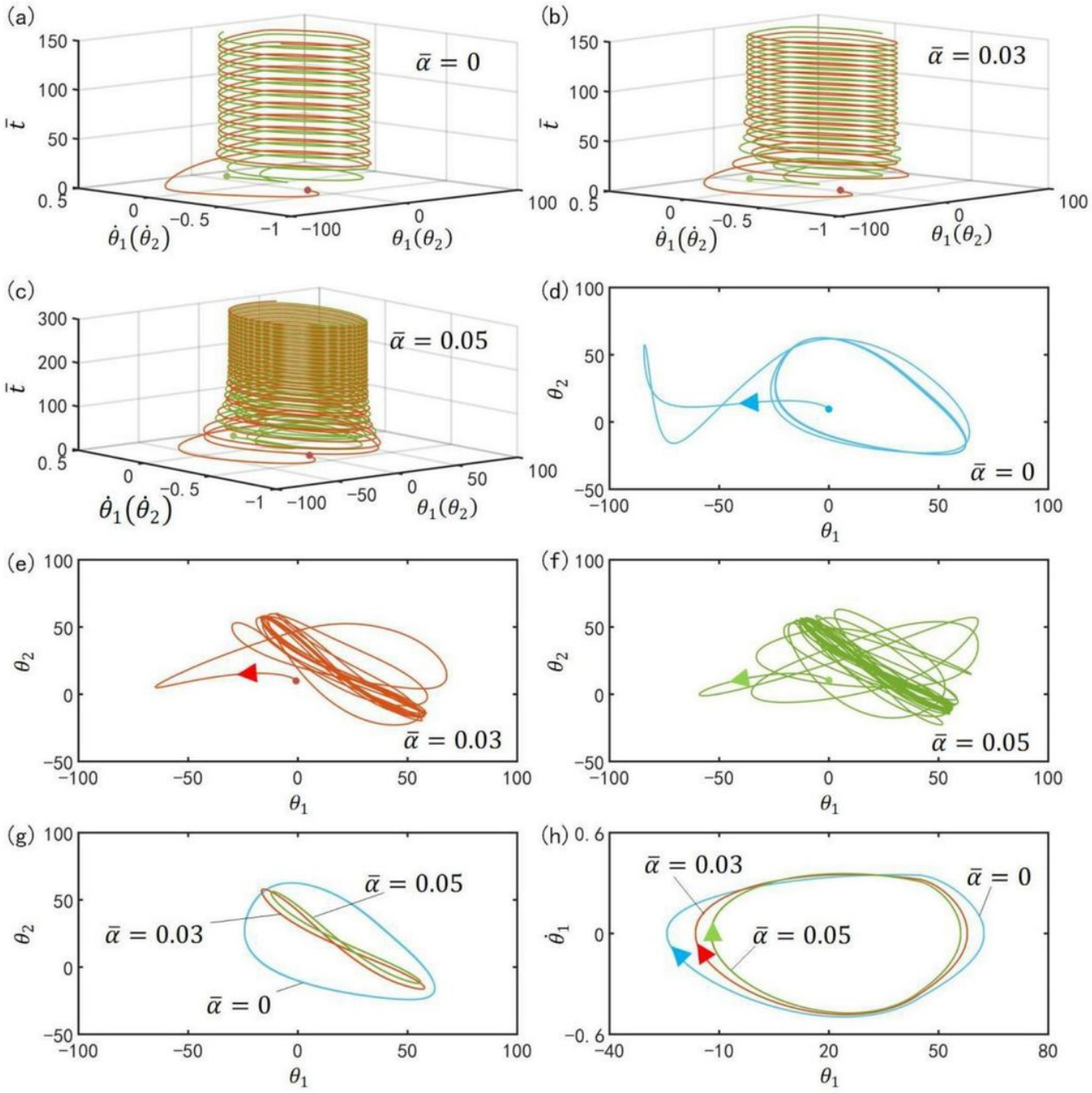

Figure 9

Please see the Manuscript PDF file for the complete figure caption